Supporting Information: Structural Characterization of Molybdenum Oxide Nanoclusters Using Ion Mobility Spectrometry–Mass Spectrometry and Infrared Action Spectroscopy

Mateusz Marianski,[†,¶] Jongcheol Seo,[†,¶] Eike Mucha,[†] Daniel A. Thomas,[†] Sabrina Jung,[†] Robert Schlögl,[†,‡] Gerard Meijer,[†] Annette Trunschke,[*,†] and Gert von Helden[*,†]

†*Fritz-Haber-Institut der Max-Planck-Gesellschaft, Faradayweg 4-6, D-14195 Berlin, Germany*

‡*Max-Planck-Institut für Chemische Energiekonversion, Stiftstrasse 34-36, D-45470 Mülheim an der Ruhr, Germany*

¶*Contributed equally to this work*

E-mail: trunschke@fhi-berlin.mpg.de; helden@fhi-berlin.mpg.de

Contents

1 Computational details

The calculations have been performed with the all-electron numeric atom-centered orbitals code FHI-aims[1] using the generalized gradient approximation exchange-correlation PBE functional[2] augmented with the Tkatchenko-Scheffler[3] scheme (vdW^{TS}) to correct for long-range van der Waals interactions. The geometry optimizations were carried out with `tight` basis set settings. An exemplary control file including convergence criteria is attached to the SI. The harmonic vibrations calculations were performed numerically by displacing each atom by 0.0025 Å in each direction followed by the digitalization of the resulting hessian. 3N-6 positive frequencies confirmed that all optimizations yielded stable minima. All optimized structures are included in an archive file attached to the manuscript.

In the theoretical calculations of CCS using projection approximation, a dummy radius of 1.8 Å for Mo atoms was adopted. Since the Mo atom is always in a center of a tetrahedron, the adopted Mo radius has a small impact on the overall CCS. A radius of 1.1 Å and 1.51 Å was utilized for hydrogen and oxygen, respectively, as reported previously.[4]

Additional calculations for $HMo_4O_{13}^{1-}$ were performed within Gaussian 16.[5] Barrier heights for rotation of the OH rotor in methanol and $HMo_4O_{13}^{1-}$ were estimated from a coordinate scan at the B3LYP[6,7] and MP2[8,9] level of theory utilizing the def2-TZVP basis set.[10,11] The initial structure for $HMo_4O_{13}^{1-}$ was taken from optimization within the FHI-aims program and subsequently reoptimized within Gaussian 16, and the initial structure for methanol was optimized directly in Gaussian 16.

2 Arrival Time Distribution Plots

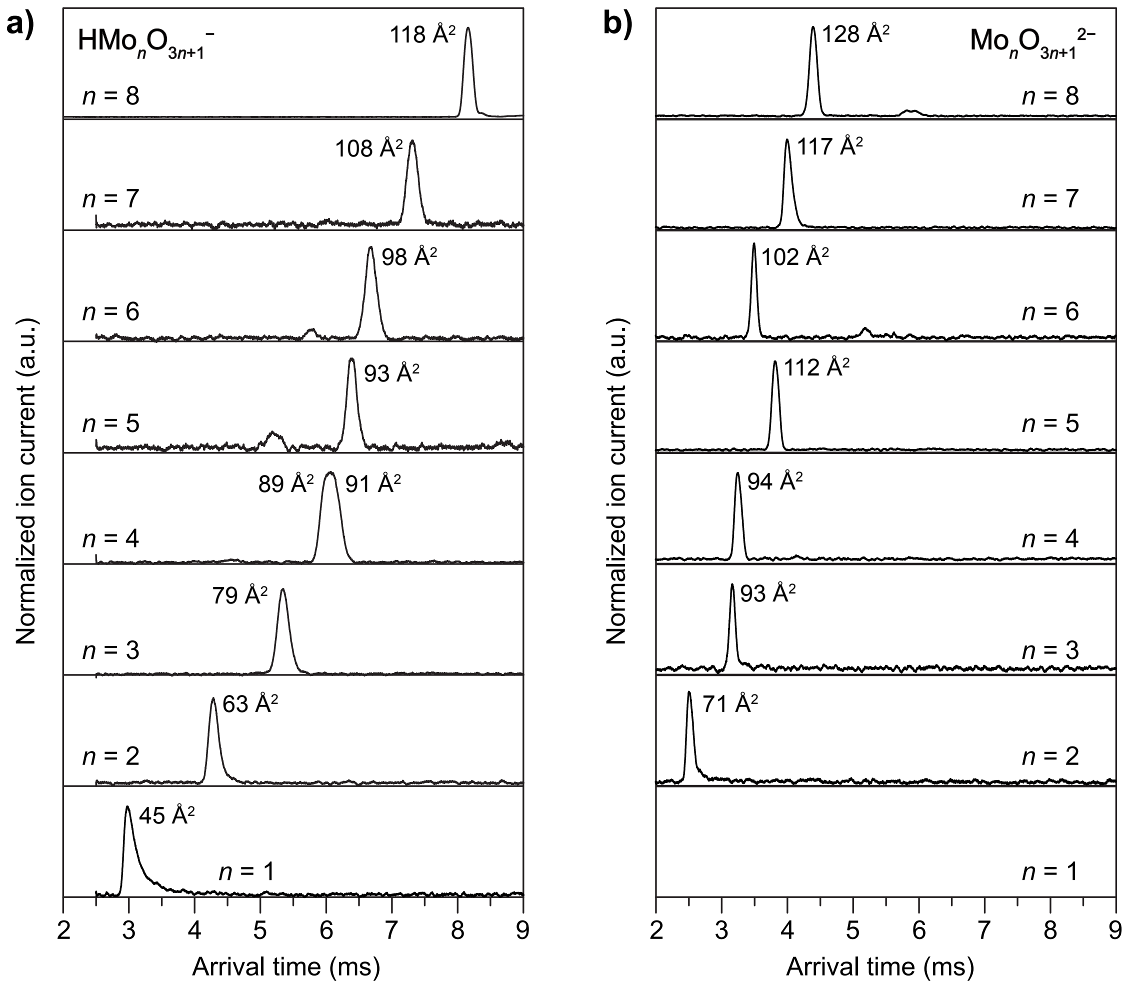

Figure S1. Arrival Time Distributions (ATD) for series of $HMo_nO_{3n+1}^{1-}$ (n = 1–8, left) and $Mo_nO_{3n+1}^{2-}$ (n = 2–8, right). With the exception of $HMo_4O_{13}^{1-}$, all ATDs show only a single feature, suggesting a single structure for each ion.

3 Theoretical CCS of $Mo_nO_{3n+1}^{2-}$ and $HMo_nO_{3n+1}^{1-}$

Table S1. Experimental and theoretical CCS for $Mo_nO_{3n+1}^{2-}$ species (n = 2–6) discussed in the manuscript. For $n = 5$, the theoretical CCS of structures shown in figure S2 are listed. All CCS values are given in units of Å^2.

n	Exp	Chain	Ring	Compact
2	71	70	-	-
3	93	92	70	-
4	94	113	92	-
5	112	136	(b) 113 (c) 110 (d) 106	-
6	102	157	139	102

Table S2. Experimental and theoretical CCS for $HMo_nO_{3n+1}^{1-}$ species (n = 1–8) discussed in the manuscript. All CCS values are given in units of Å^2.

n	Exp	Theory
1	45	47
2	63	65
3	79	83
4	90	91
5	93	97
6	98	101
7	108	114
8	118	125

4 Additional Theoretical IR Spectra for $Mo_5O_{16}^{2-}$

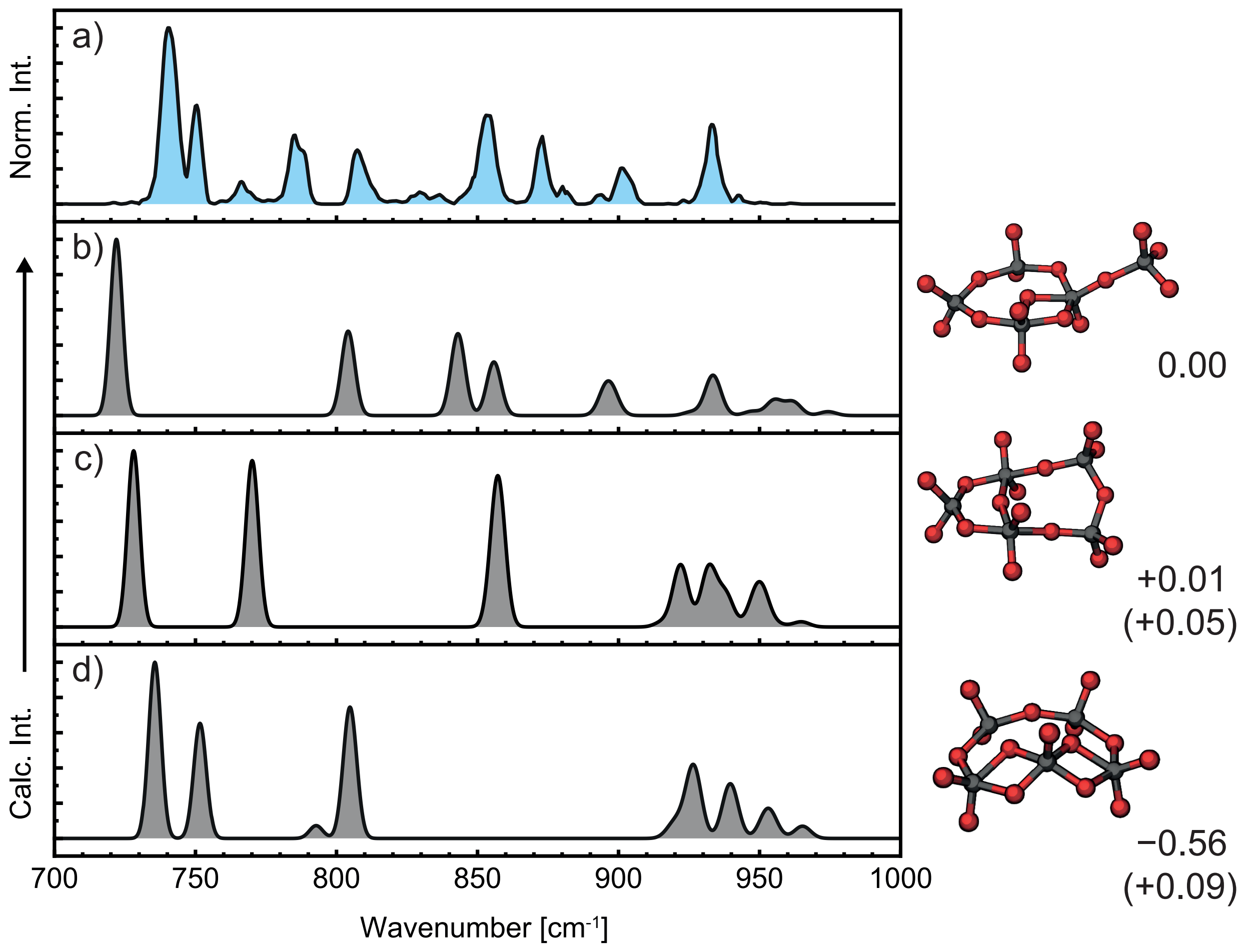

Figure S2. Theoretical IR spectra for calculated low-energy structures of $Mo_5O_{16}^{2-}$ (gray, b–d) compared to the experimental spectrum collected in He nanodroplets (blue, a). The structures corresponding to each theoretical spectrum are shown at right. The relative energies of the structures in kcal mol^{-1} are also shown at right, with the relative energy following zero-point correction shown in parentheses.

5 Additional Theoretical IR Spectra for $Mo_7O_{22}^{2-}$

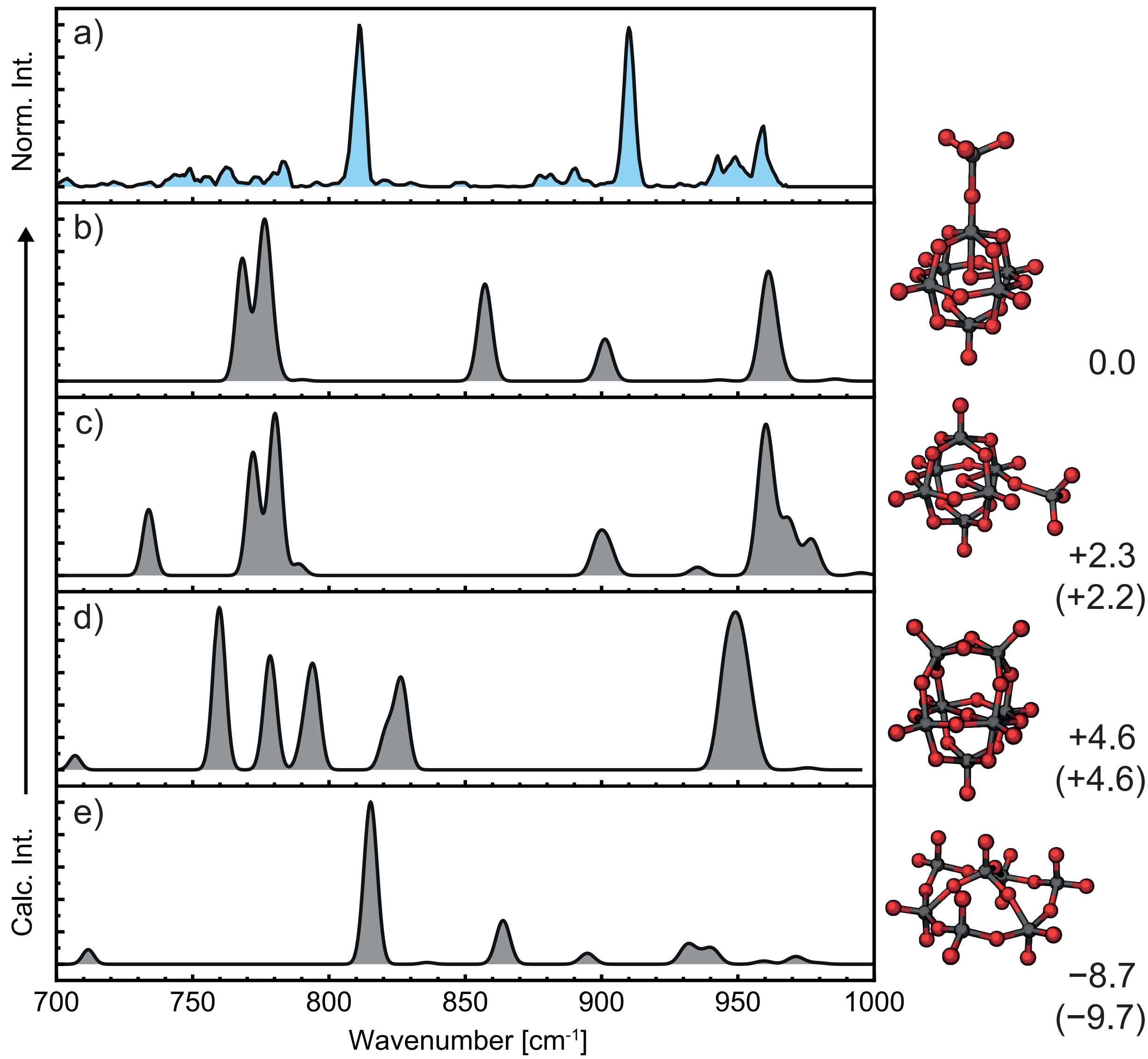

Figure S3. Theoretical IR spectra for calculated low-energy structures of $Mo_7O_{22}^{2-}$ (gray, b–e) compared to the experimental spectrum collected in He nanodroplets (blue, a). The structures corresponding to each theoretical spectrum are shown at right. The relative energies of the structures in kcal mol^{-1} are also shown at right, with the relative energy following zero-point correction shown in parentheses.

6 IRMPD and Theoretical IR Spectra for $Mo_8O_{25}^{2-}$

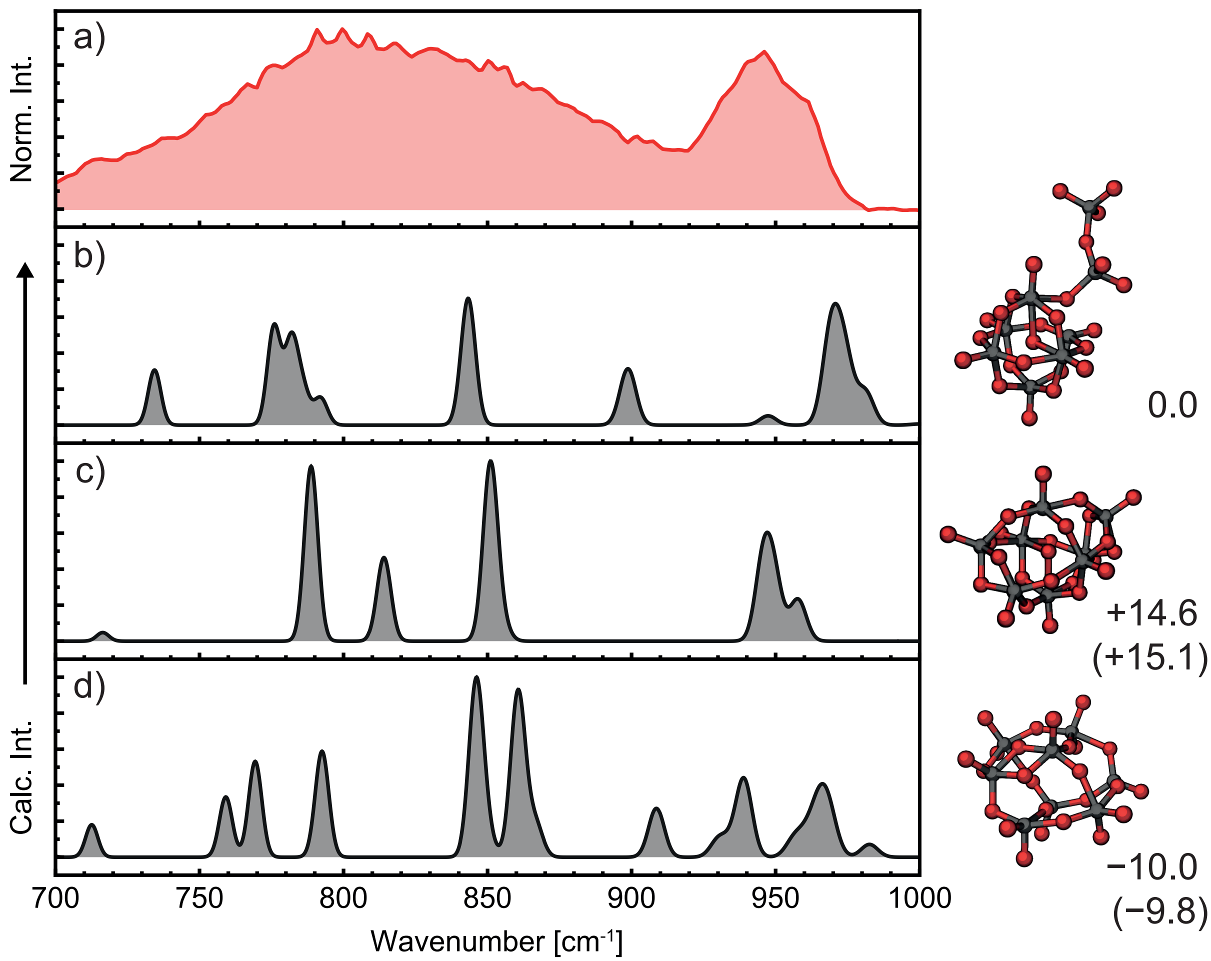

Figure S4. Theoretical IR spectra for calculated low-energy structures of $Mo_8O_{25}^{2-}$ (gray, b–d) compared to the experimental spectrum collected by IRMPD (red, a). The structures corresponding to each theoretical spectrum are shown at right. The relative energies of the structures in kcal mol^{-1} are also shown at right, with the relative energy following zero-point correction shown in parentheses.

7 Relative Energy and CCS of $Mo_8O_{25}^{2-}$ Structures

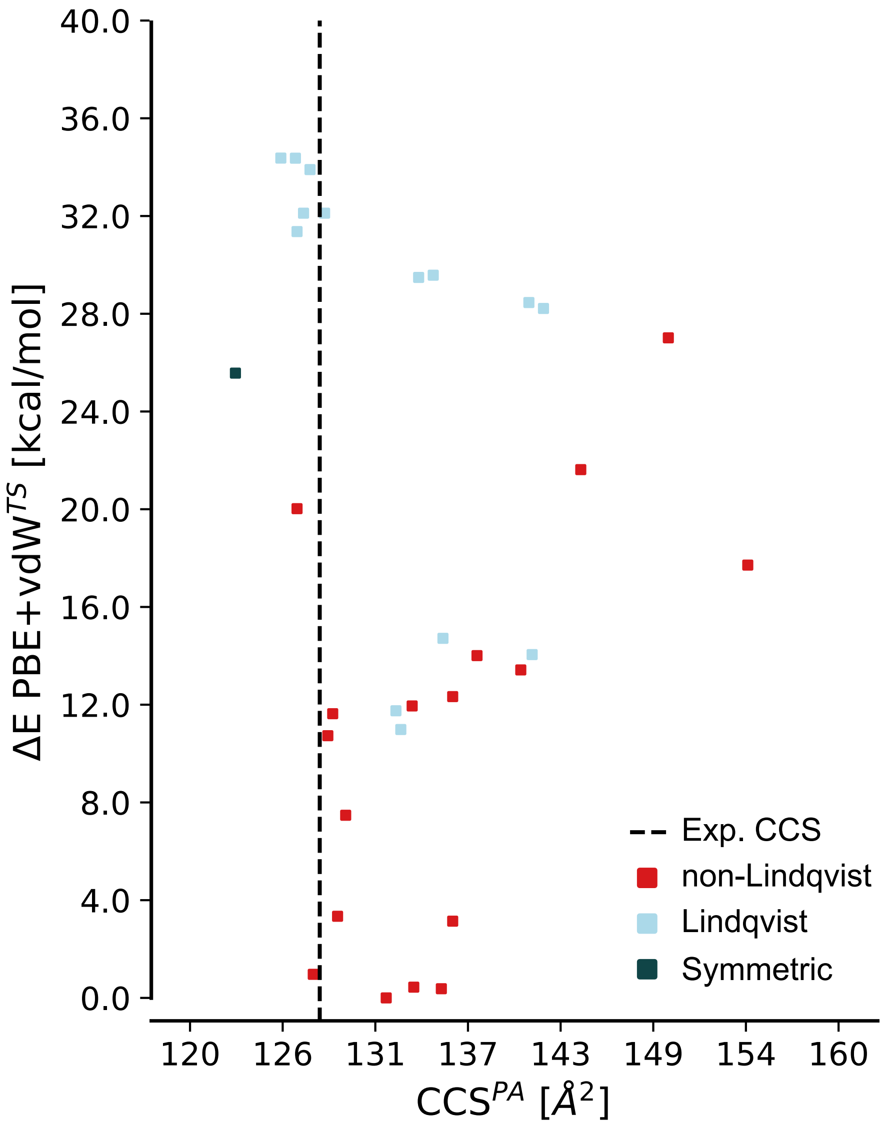

Figure S5. Plot of relative energy (PBE + vdW^{TS}) vs. CCS for theoretical structures of $Mo_8O_{25}^{2-}$. The dashed line shows the experimental CCS value, and colored boxes denote calculated values for modified Lindqvist (blue), non-Lindqvist (red), and symmetric structures (green). Expanded, non-Lindqvist structures are predicted to be the most stable category of structure and also show good agreement with the epxerimental CCS value.

References

(1) Blum, V.; Gehrke, R.; Hanke, F.; Havu, P.; Havu, V.; Ren, X.; Reuter, K.; Scheffler, M. Ab Initio Molecular Simulations with Numeric Atom-Centered Orbitals. *Comput. Phys. Commun.* **2009**, *180*, 2175–2196.

(2) Perdew, J. P.; Burke, K.; Ernzerhof, M. Generalized Gradient Approximation Made Simple. *Phys. Rev. Lett.* **1996**, *77*, 3865–3868.

(3) Tkatchenko, A.; Scheffler, M. Accurate Molecular Van Der Waals Interactions from Ground-State Electron Density and Free-Atom Reference Data. *Phys. Rev. Lett.* **2009**, *102*, 73005.

(4) Wyttenbach, T.; Witt, M.; Bowers, M. T. On the Stability of Amino Acid Zwitterions in the Gas Phase: The Influence of Derivatization, Proton Affinity, and Alkali Ion Addition. *J. Am. Chem. Soc.* **2000**, *122*, 3458–3464.

(5) Frisch, M. J.; Trucks, G. W.; Schlegel, H. B.; Scuseria, G. E.; Robb, M. A.; Cheeseman, J. R.; Scalmani, G.; Barone, V.; Petersson, G. A.; Nakatsuji, H. et al. Gaussian 16 Revision A.01. 2016; Gaussian Inc. Wallingford CT.

(6) Becke, A. D. Density-Functional Thermochemistry. III. The Role of Exact Exchange. *J. Chem. Phys.* **1993**, *98*, 5648–5652.

(7) Stephens, P. J.; Devlin, F. J.; Chabalowski, C. F.; Frisch, M. J. Ab Initio Calculation of Vibrational Absorption and Circular Dichroism Spectra Using Density Functional Force Fields. *J. Phys. Chem.* **1994**, *98*, 11623–11627.

(8) Møller, C.; Plesset, M. S. Note on an Approximation Treatment for Many-Electron Systems. *Phys. Rev.* **1934**, *46*, 618–622.

(9) Bartlett, R. J. Many-Body Perturbation Theory and Coupled Cluster Theory for Electron Correlation in Molecules. *Annu. Rev. Phys. Chem.* **1981**, *32*, 359–401.

(10) Weigend, F.; Ahlrichs, R. Balanced Basis Sets of Split Valence, Triple Zeta Valence and Quadruple Zeta Valence Quality for H to Rn: Design and Assessment of Accuracy. *Phys. Chem. Chem. Phys.* **2005**, *7*, 3297–3305.

(11) Weigend, F. Accurate Coulomb-Fitting Basis Sets for H to Rn. *Phys. Chem. Chem. Phys.* **2006**, *8*, 1057–1065.